Geophysical Research Letters

RESEARCH LETTER
10.1029/2025GL116613

# How Spatially Variable Are Tropical and Subtropical Convective Environments?

**Itinderjot Singh**[1], **Jennie Bukowski**[1], **Peter J. Marinescu**[1], **Leah D. Grant**[1], and **Susan C. van den Heever**[1]

[1]Department of Atmospheric Science, Colorado State University, Fort Collins, CO, USA

**Key Points:**

- Near-surface winds vary more sharply across space (shorter correlation lengths) than moisture or temperature over land
- Tropical oceanic convective environments have the smallest magnitudes of spatial variability in near-surface moisture and temperature
- Tropical oceanic convective environments show greater magnitudes of moisture variability compared to land over a wide range of length scales

**Supporting Information:**

Supporting Information may be found in the online version of this article.

**Correspondence to:**

I. Singh,
I.Singh@colostate.edu

**Citation:**

Singh, I., Bukowski, J., Marinescu, P. J., Grant, L. D., & van den Heever, S. C. (2025). How spatially variable are tropical and subtropical convective environments? *Geophysical Research Letters*, *52*, e2025GL116613. https://doi.org/10.1029/2025GL116613

Received 23 APR 2025
Accepted 7 NOV 2025

**Author Contributions:**

**Conceptualization:** Itinderjot Singh
**Formal analysis:** Itinderjot Singh
**Funding acquisition:** Susan C. van den Heever
**Methodology:** Itinderjot Singh, Jennie Bukowski, Peter J. Marinescu, Leah D. Grant, Susan C. van den Heever
**Project administration:** Susan C. van den Heever
**Software:** Itinderjot Singh
**Writing – original draft:** Itinderjot Singh
**Writing – review & editing:** Susan C. van den Heever



**Abstract** Quantifying horizontal spatial variability in high-resolution simulated convective environments is key to improving parameterizations for coarser models, accurately comparing models and observations, and understanding the physical processes driving this variability. Here, we characterize horizontal spatial variability in a large sample of simulated tropical and subtropical convective environments using structure functions. Near the surface, horizontal wind is spatially rougher (smaller decorrelation lengths) than moisture and temperature over land for length scales between 10 and 100 km. At 500 hPa, tropical oceanic convective environments display smoother moisture fields compared to temperature and wind at the same scales. Besides roughness, we also compute absolute magnitudes of variability at different length scales. Across simulations, tropical oceanic environments show the smallest magnitudes of surface temperature and moisture variability. However, at 500 hPa, the tropical oceanic simulations show greater moisture variability magnitudes compared to land cases, suggesting the influence of strong, large-scale moisture gradients over tropical oceans.

**Plain Language Summary** The spatial variability of storm environments in weather and climate models can strongly affect short-term predictability of thunderstorms as well as climate projections. Here, we analyze how environmental temperature, moisture, wind, instability, and surface heat and moisture exchange, vary across space using high-resolution simulations of tropical and subtropical storms. We use statistical tools to measure the texture of these fields (how smooth or rough these fields are and hence how gently or abruptly they change in space) at different heights in the atmosphere and in different environments. We find that the surface wind field has a more uneven texture than temperature and moisture over land. The absolute magnitude of mid-level moisture variability is greater over tropical oceans than over land for a large range of length scales. Some surface variables show distinct spatial patterns tied to local features like terrain. These differences mean that a one-size-fits-all model resolution will not work for all variables. Our results can help improve weather models and observing systems by showing how to represent smaller-scale variability when it can't be directly resolved and by estimating how far apart should we place our instruments in the field to sufficiently capture the details of a given variable.

## 1. Introduction

Depending on the spatial resolution and area, a scene containing deep moist convection could contain spatial scales of variability corresponding to planetary boundary layer circulations, storm updrafts, cold pools, gravity waves, meso- and synoptic-scale boundaries, amongst other features (Fabry, 2006; Kiemle et al., 2017; Naumann & Kiemle, 2020; Smith et al., 2005). Quantifying the variability in simulated or observed geophysical fields as a function of distance is important for several reasons. First, poor representation of the sub-grid scale variability in thermodynamic variables can lead to errors in the initiation and growth of deep convection, negatively affecting short-term predictability and climate projections (e.g., Tompkins, 2002; Tompkins & Berner, 2008; Zhang et al., 2003). Knowledge of the scaling behavior of sub-grid variability is also essential for developing scale-aware and stochastic parameterizations (Berner et al., 2017; Schemann et al., 2013). Second, knowing how rapidly a convective environment changes from one location to another can help estimate the appropriate density of measurements necessary in the field (e.g., Madaus & Hakim, 2016). Relatedly, it can assist in better gauging the error when ascribing environmental profiles to storms. This is important as many idealized studies initiate convection in homogenous environments using a single sounding. Third, the scales of variability serve as useful diagnostics when comparing model output with other models or observations (Freischem et al., 2024; Grant et al., 2024; Kahn et al., 2011; Marzban & Sandgathe, 2009; Selz et al., 2017). Finally, quantifying the patterns of

variability across convective environments can help to identify potential universal scalings (Tsonis et al., 1999) and understand the physical processes driving this variability.

Several studies have characterized spatial variability in moisture and temperature using both observations and numerical simulations (e.g., Davison et al., 2013; Kahn et al., 2011; Kiemle et al., 2017; Sherwood, 1996; Stevens et al., 2019). Kiemle et al. (2017) used lidar data over the wintertime tropical Atlantic Ocean around Barbados to show that dominant length scales of variability for humidity are between 300 and 600 km in the shallow cloud and marine boundary layers. They attributed this variability to the convective redistribution of moisture. They also noted that scaling exponents near the base of the subsidence inversion show breaks on the order of 10–30 km, suggesting a complex spatial structure of the water vapor field. More recently, P. J. Marinescu et al. (2024) used high-resolution numerical simulations to show that significant sub-grid variability exists at typical reanalysis grid spacing lengths, and that surface winds, convective available potential energy (CAPE), and mid-level moisture are the most variable among the convective parameters they tested.

Prior studies were often restricted to a small set of convective environments or a small range of length scales. This study aims to characterize the scale dependence of horizontal variability in simulated convective environments spanning convective morphologies from scattered thunderstorms to mesoscale convective systems, throughout the tropics and subtropics. These simulations have been conducted in support of the National Aeronautics and Space Administration (NASA) Investigation of Convective Updrafts (INCUS) mission (Dolan et al., 2023; Prasanth et al., 2023; van den Heever, 2021). We use structure functions and variograms to address two primary questions:

1. How do the patterns and magnitudes of spatial variability of moisture, temperature, winds, surface fluxes and CAPE differ (a) amongst the variables, (b) between maritime and continental convective environments, and (c) between tropical and subtropical convective environments in high-resolution numerical simulations?
2. What are the predominant length scales of variability for these simulated environmental variables?

## 2. Methods

### 2.1. Numerical Simulations

The simulations analyzed in this study are conducted with the Regional Atmospheric Modeling System (RAMS, Cotton et al., 2003; Saleeby & van den Heever, 2013; van den Heever et al., 2023). The outermost grids (G1) of all simulations have a horizontal grid spacing of 1.6 km and 232 vertical levels, with a maximum vertical grid spacing of 125 m. Additional details about the model setup are given in P. J. Marinescu et al. (2024). Figure 1 shows examples of the near-surface water vapor mixing ratios at one time for all the simulations, along with a characterization of the simulated convective morphology and environment. While these simulations include two additional one-way nested grids, here we only analyze the largest grid (G1) to quantify variability across a wider range of length scales. The size of G1 varies from $784 \times 784$ km$^2$ for the Argentina simulations (Figures 1j and 1k) to $2{,}222 \times 1{,}667$ km$^2$ for the Brazil simulations (Figures 1g and 1h). Table S1 in Supporting Information S1 shows the names of the simulations, their grid sizes, and dominant convective morphologies. While this study focuses on the RAMS model simulations, we also simulated these cases with the Weather Research and Forecasting (WRF, Skamarock et al., 2019) model with two different microphysics schemes. The results presented in this paper are consistent across all three modeling frameworks (see Supporting Information S1).

### 2.2. Quantifying Horizontal Spatial Variability: Structure Functions and Variograms

Figures 2a and 2b show two fields with different spatial textures: field B is smoother than field A. However, both fields have the same mean ($\mu = 0$) and variance ($\sigma^2 = 0.25$), precluding us from using variance or standard deviation to contrast their spatial structure. Instead, we use structure functions to quantify the spatial variability in these fields. The $q$th-order structure function ($\widehat{S}_q$) for a two-dimensional field $f(\boldsymbol{x})$ is estimated by computing the average of the $q$th power of the magnitude of difference of values (hereafter called increments) for all pairs of points separated by some distance, $d$ (called spatial lag or lag distance), that is,

10.1029/2025GL116613

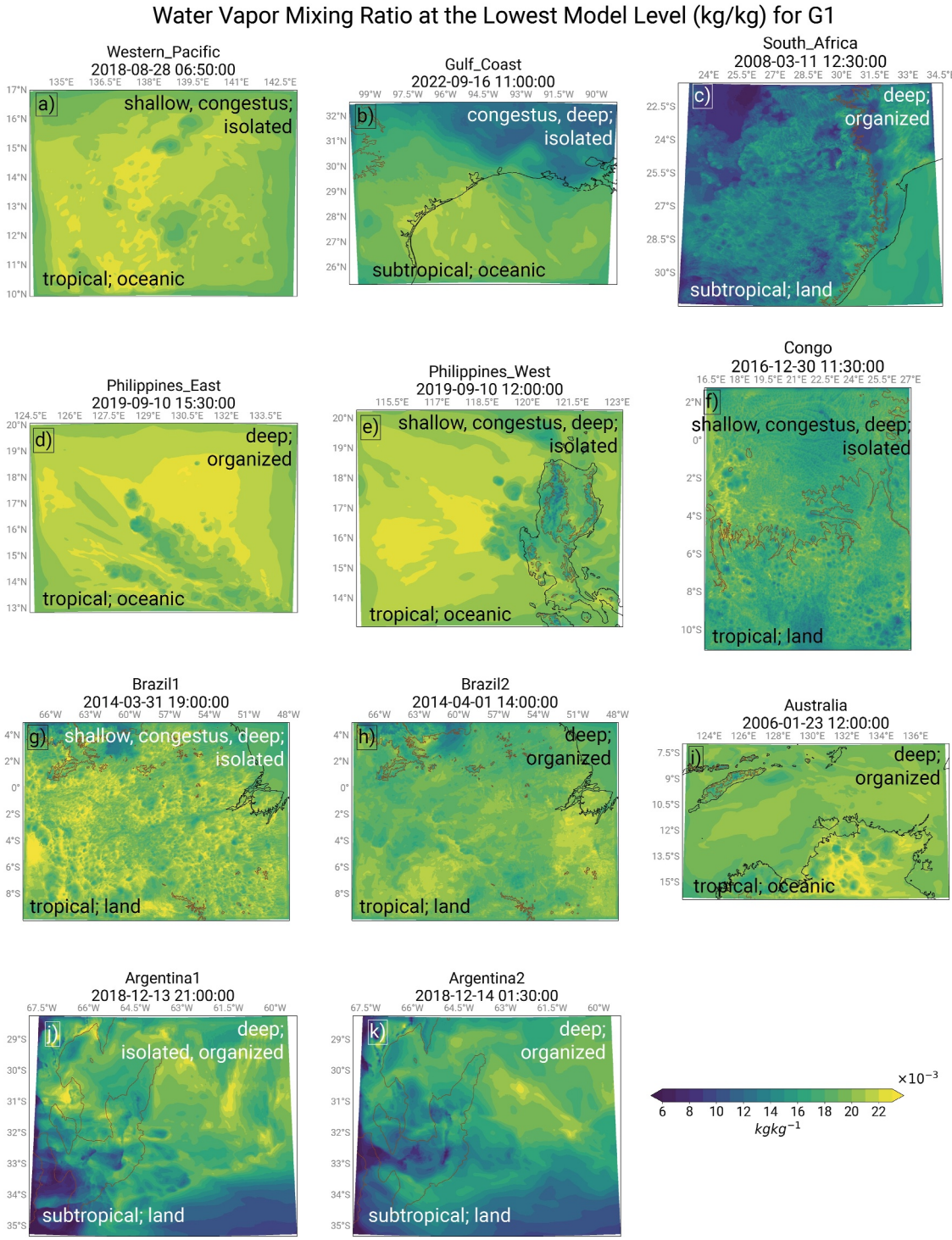


**Figure 1.** The horizontal structure of water vapor mixing ratio varies across convective regimes and tropical and subtropical regions. Shown here are examples of the water vapor mixing ratios (kg/kg) at the lowest model level at one time for the simulations used in this study. The 500-m terrain height contour is shown in brown.

$$\widehat{S_q}(d) = \frac{1}{N(d)} \sum_{\substack{i \neq j \\ |\boldsymbol{x}_i - \boldsymbol{x}_j| = d}}^{N} |f(\boldsymbol{x}_i) - f(\boldsymbol{x}_j)|^q \quad (1)$$

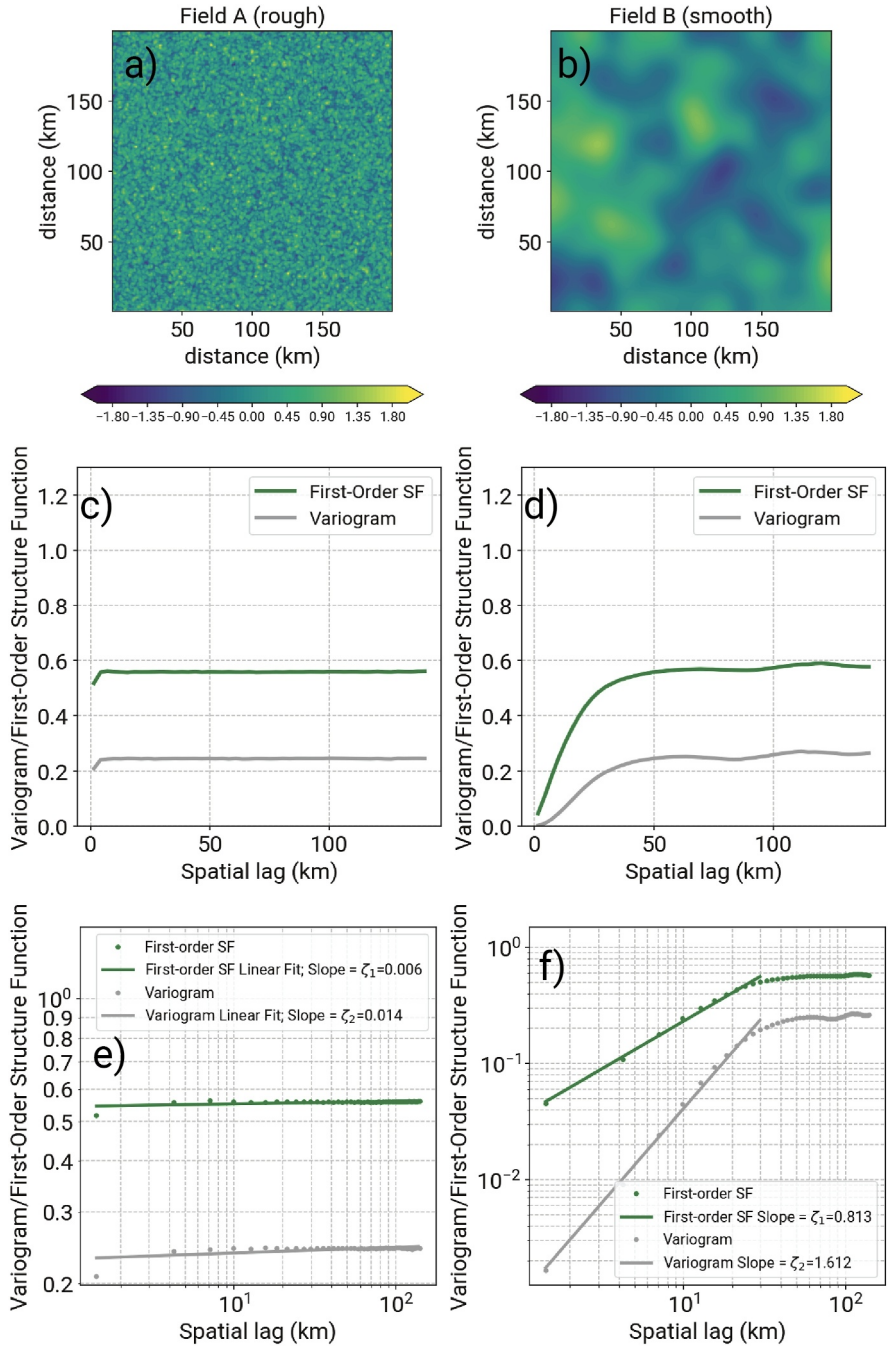


**Figure 2.** (a, b) Two fields with the same mean ($\mu = 0$) and variance ($\sigma^2 = 0.25$). Note the difference in the texture of the two fields; field B is much smoother than field A. (c, d) First-order structure functions (SF) and variograms versus spatial lag (km) for fields A and B, respectively. (e, f) As in (c, d), respectively, but in log-log space; linear regression fits to the variograms and first-order SF along with the slopes of the fitted lines are also shown.

Here, $N$ is the number of pairs of points separated by lag distance $d$. Figures 2c and 2d show first-order structure function and variograms (which are simply second-order structure functions divided by 2) for fields A and B, respectively. Both the first-order structure function ($q = 1$) and the variogram ($q = 2$) provide a statistical measure of how the similarity between two points in the domain changes as the distance between them increases. For detailed definitions of structure functions and variograms, please refer to Sections S1.1 and S1.2 in Supporting Information S1, respectively.

For field A, both the first-order structure function and the variogram are essentially constant with lag distance (Figure 2c). For field B, however, the first-order structure function and variogram (Figure 2d) look quite different; these curves, representing the magnitude of variability at a given spatial scale, first rise and then plateau after ∼30 km. This points to the predominance of features of size ∼30 km in field B. The lag distance at which a variogram levels off is referred to as the variogram *range* (∼30 km in this case), and the value it attains as it levels off is called its *sill* (0.25 in this case; the sill of the variogram approaches variance under some assumptions). Figures 2e and 2f show linear regression fits in log-log space to the structure functions and variograms for fields A and B, respectively. The slopes of these linear fits, also called structure function exponents, condense the information in the curve across multiple lag distances into one scalar. $\zeta_1$, the slope of the first-order structure function, is an approximation of the Hurst exponent (Hurst, 1956) and characterizes the texture (rough or smooth) of the data; low values of $\zeta_1$ imply more texturally rough data, meaning the field changes more abruptly and frequently over space. $\zeta_2$, the slope of the variogram or second-order structure function (under some assumptions), is related to the slope of the power spectrum of the field (Khintchine, 1934; Lewis et al., 2004); large values of $\zeta_2$ (equivalently, steep slopes of the power spectrum) can imply there is little variance at small spatial scales.

Similar to the above example, we compute structure functions for environmental moisture, temperature, and winds near the surface and at 500 hPa, as well as for surface fluxes and CAPE, from our high-resolution numerical simulations. These variables were chosen given their significance in determining convective outcomes (e.g., Schulte et al., 2024; Storer & Posselt, 2019). Here, the environment at a given altitude is defined as grid points where total condensate mixing ratio is less than $10^{-4}$ g/kg; we ignore cloudy points for structure function computation. Please refer to Section S1.3 in Supporting Information S1 for more details regarding calculations of structure functions for the environmental grid points. While we estimate structure functions for orders one through five (Figure S1 in Supporting Information S1), we only present the exponents and curves for the first-order structure function and variogram as they have more intuitive interpretations. Additionally, while the magnitudes of the structure functions of different orders differ from each other (Figure S1 in Supporting Information S1), they largely preserve the relative variability across simulations for all spatial scales. We choose variograms (second-order structure function) as the primary tool for assessing absolute magnitudes of variability at different scales, making comparisons across simulations, and obtaining characteristic length scales of variability due to their abundant use in the literature, their straightforward relationship with variance, and the existence of a variety of theoretical models for retrieval of the variogram ranges (Chilès & Delfiner, 2012).

Thus, we distinguish between two aspects of spatial variability: variability magnitude and roughness. Variability magnitude for a given spatial scale refers to the absolute strength of spatial increments, quantified by values of the variogram at that lag distance. In contrast, roughness refers to the scale dependence of those increments, quantified by the slope of the first-order structure function for given range of lag distances. Importantly, these capture distinct features: a field may have large increments (high variability magnitude) but still be smooth (steep slope), or it may be jagged or rough (shallow slope) despite smaller overall variability. Moreover, roughness is closely related to the spatial correlation scale: rougher fields (shallower slopes) tend to correlate over shorter distances, while smoother fields (steeper slopes) retain spatial coherence over longer distances. We can compare roughness across different variables because the metric of roughness (the slope of first-order structure function) is dimensionless. We cannot compare variability magnitudes across variables as they have different units, for example, $g^2/kg^2$ versus $K^2$.

## 3. Results and Discussion

### 3.1. Structure Function Exponent Analysis

Figure 3 shows the first- and second-order structure function exponents for near-surface and 500 hPa environmental water vapor mixing ratio, temperature, and wind speed. We compute these exponents for length scales of 10–100 km, roughly within meso-$\beta$ scales. The surface moisture is the roughest in Congo and Brazil1 simulations (see also Figures 1f and 1g). This makes sense as these simulations feature land environments with daytime convective boundary layer, heterogenous surface, and scattered, isolated convection. Additionally, in general, marine tropical convective environments tend to have larger values of $\zeta_1$ compared to tropical land environments, implying smoother surface moisture fields with longer correlation lengths in marine tropical environments.

For all 11 simulations, for surface water vapor, we obtain $\zeta_1 = 0.49 \pm 0.16$ (mean ± standard deviation) and $\zeta_2 = 0.85 \pm 0.31$. The mean $\zeta_2$ is greater than the theoretical second order exponent (2/3), indicating that there

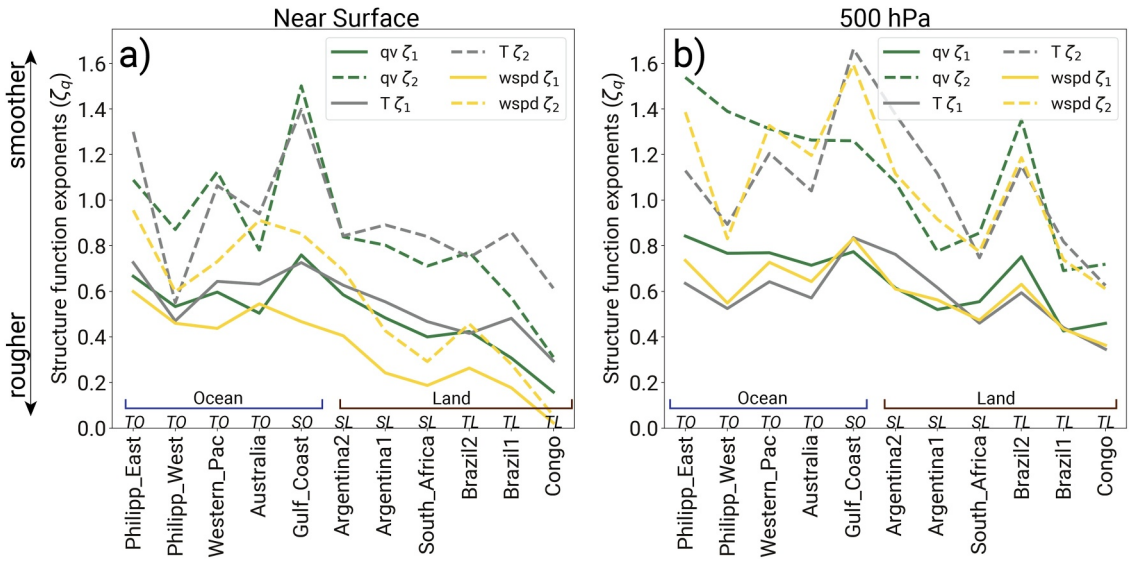


**Figure 3.** Values of first- and second-order structure function exponents for length scales of 10–100 km for water vapor mixing ratio, temperature, and wind speed (a) near surface and (b) at 500 hPa for all simulations. Italicized labels above the *x*-axis indicate tropical (*T*) or subtropical (*S*) and oceanic (*O*) or land (*L*) environments. Note that some oceanic environments contain land in the domain.

may be loss of variance at small scales in some of the numerical simulations (Kahn et al., 2011; Nastrom et al., 1986; Tung & Orlando, 2003). Similarly, for water vapor mixing ratios at 500 hPa (free troposphere), we obtain $\zeta_1 = 0.65 \pm 0.14$ and $\zeta_2 = 1.11 \pm 0.3$. The 500 hPa water vapor $\zeta_1$ is larger than that for the near-surface values, implying that environmental water vapor has a smoother texture at midlevels than at the surface. These values are within the range of observations taken in three field campaigns within areas without active convection (but in the vicinity of convection) in the free troposphere: $\zeta_1 = 0.63 \pm 0.10$ and $\zeta_2 = 1.19 \pm 0.19$ (Table 2 in Fischer et al. (2013)). While there are caveats to comparing structure function exponents between observations and simulated data (differing atmospheric regimes, sampling strategies, altitude, etc.), a rudimentary comparison such as this ensures that the spatial variability in our numerical simulations is within the bounds of observations.

Based on the values of $\zeta_1$ in Figure 3a (Figures S2 and S4 in Supporting Information S1 for WRF), surface wind speed is rougher (shorter correlation lengths) compared to moisture and temperature fields for length scales of 10–100 km for land environments. However, at 500 hPa, water vapor is the smoothest and temperature field is the roughest over tropical oceanic convective environments for these length scales. The differing spatial textures and correlation length scales among variables imply that a model resolution or an observation network sufficient for capturing one variable, such as near-surface temperature, may be inadequate for others, like near-surface wind speed. Moreover, the representativeness of a simulated or radiosonde profile of a storm environment varies with altitude and depends on the specific variable considered.

### 3.2. Variograms for G1

#### 3.2.1. Water Vapor Mixing Ratio

Figures 4a–4f show the variograms of water vapor mixing ratio, temperature, and wind speed at the surface and 500 hPa. The near-surface water vapor variograms (Figure 4a) are broadly separated into two groups: subtropical (Argentina1, Argentina2, South_Africa, and Gulf_Coast) and tropical simulations (Congo, Brazil1, Brazil2, Philippines_West, Philippines_East, Western_Pacific, and Australia), with subtropical convective environments having larger variogram values at all lag distances and hence larger horizontal spatial variability magnitudes than their tropical counterparts. Among the tropical simulations, entirely marine convective environments (Philippines_East and Western_Pacific) tend to have lower surface moisture variability compared to convective environments over land (Brazil1, Brazil2, and Congo) for all lag distances. Greater moisture variability over land can be explained by steeper terrain, topography-related mechanical and thermal circulations, stronger boundary layer circulations, stronger cold pools, and other land surface inhomogeneities including soil moisture. Figure 4j shows the ranges of the theoretical variogram models fitted to the empirical variograms shown in Figures 4a–4i. As

10.1029/2025GL116613

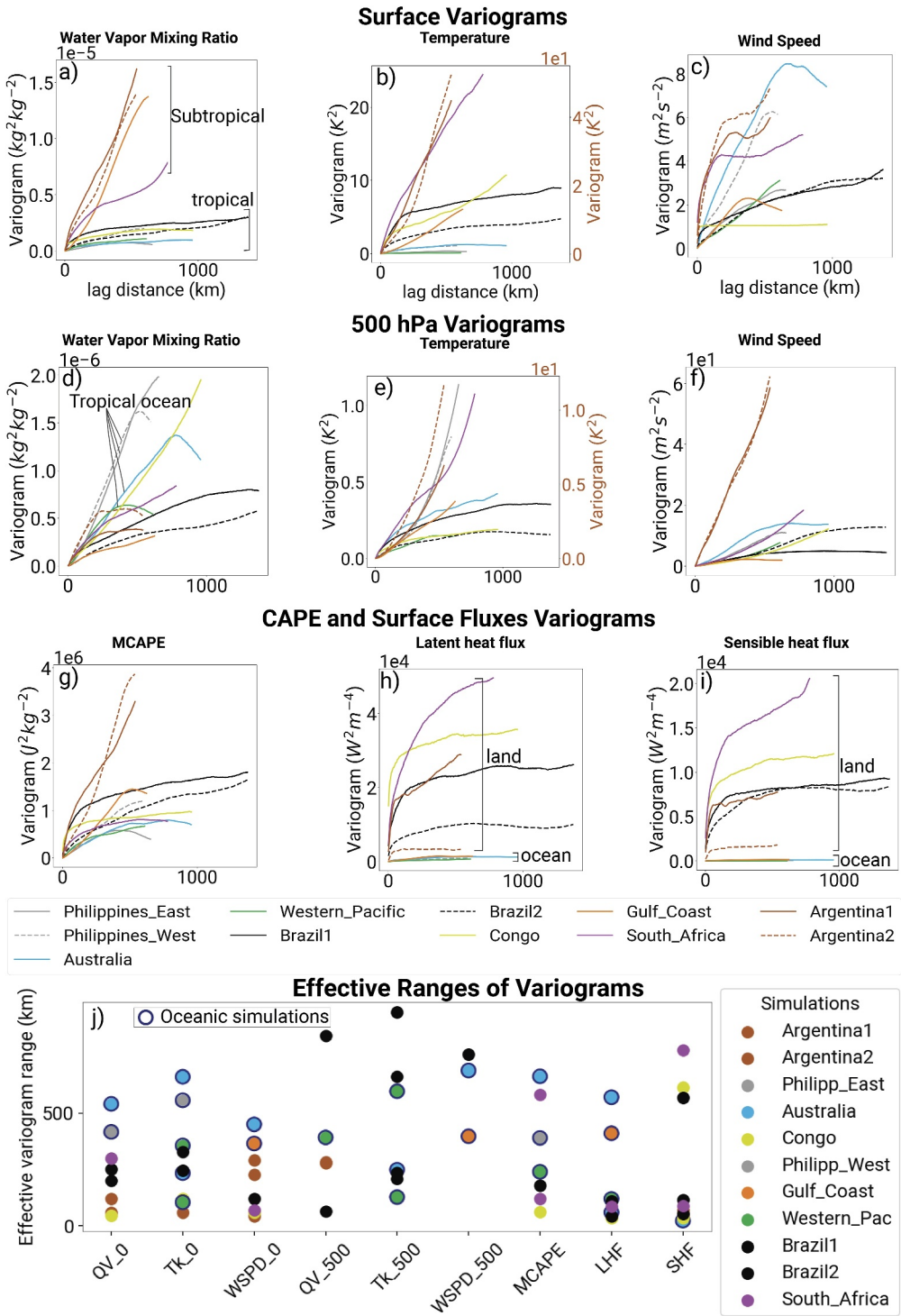


**Figure 4.** Variograms for water vapor mixing ratio, temperature, and (a–c) wind speed at the surface and at (d–f) 500 hPa; (g–i) variograms for Maximum convective available potential energy, latent heat flux, and sensible heat flux. (b, e) Note that in the temperature variograms, the curves for Argentina1 and Argentina2 correspond to the brown twin *y*-axis on the right (brown). Panel (j) shows length scales of variability (effective variogram ranges, km) for the nine variables for all the simulations. The circled data points in panel (j) indicate oceanic environments. Note that some simulations contain multiple length scales of variability for certain variables. Some variograms do not have retrievable length scales associated with them: the variability keeps increasing with distance.

mentioned previously, these ranges can be interpreted as the length scales of variability present in these fields. The length scales of variability in near-surface water vapor vary from about 50 to 300 km for land environments and 400 to 600 km for oceanic environments in our simulations (Figure 4j). These results are similar to Kiemle et al. (2017), who analyzed water vapor variability in the lowest 4 km of the tropical Atlantic Ocean east of Barbados and found regions of greater moisture with sizes between 300 and 600 km. We speculate that these length scales correspond to the redistribution of moisture by large convective systems over oceans, whereas the shorter length scales over land can be interpreted as scales of variability in convective environments arising from topographical and other land surface effects.

At 500 hPa (Figure 4d), the subtropical-tropical separation seen in the surface water vapor variograms no longer exists. In fact, the 500-hPa moisture variability in tropical oceanic environments (Philippines_West, Philippines_East, Western_Pacific, and Australia) generally exceeds that in most tropical and subtropical land simulations over a wide range of length scales, with the two Philippines simulations exhibiting the greatest variability along all simulations. We speculate that a combination of moisture variability due to detrainment from convection near the melting layer, as well as moisture gradients associated with gravity waves, equatorial waves, and monsoonal circulations, might be responsible.

#### 3.2.2. Temperature

For surface temperature (Figure 4b), entirely marine tropical convective environments (Philippines_East and Western_Pacific) exhibit the least variability at all spatial scales, and subtropical land environments (Argentina1, Argentina2, and South_Africa) with steeper topography exhibit the greatest variability over a wide range of length scales. The rest of the environments lie between these two extremes.

At 500 hPa (Figure 4e), the greatest temperature variability still exists in subtropical land simulations, with variability in the Argentina simulations an order of magnitude larger than other simulations: this is likely a result of strong synoptic-scale temperature gradients. There is no clear distinction between tropical land and tropical oceanic convective environments. Additionally, similar to 500 hPa moisture, variability in 500 hPa temperature for Philippines_West and Philippines_East surpasses the rest of the tropical simulations, especially for scales larger than 300 km. The two observations are likely related and point toward the presence of large-scale gradients in temperature and moisture in these simulations.

#### 3.2.3. Wind Speed

Generally, the subtropical continental winds (Argentina1, Argentina2, and South_Africa) show greater variability at the surface (Figure 4c). The surface wind speed variograms of land environments (Congo, South_Africa, Argentina1, and Argentina2) show a relatively sharp transition from the rising portion to the sill, with variogram ranges between 60 and 300 km (Figure 4j). Such variograms have strong spatial decorrelation at specific scales, pointing to the increased role of local processes in producing variability. It's likely that the variability in surface wind speeds in convective environments over land is at least partly dominated by topography and other land surface characteristics constant in space and time. This is different from oceanic environments, where variability in surface wind speeds is primarily dictated by large-scale pressure gradients and storm inflow/outflows. The length scales of variability for surface winds exceed 300 km for oceanic simulations.

At 500 hPa (Figure 4f), the two Argentina simulations exhibit the greatest variability, likely due to strong synoptic-scale pressure gradients combined with the effects of intense deep convection in the vicinity. There is no clear distinction between tropical land and ocean environment. The length scales of variability for wind speeds at 500 hPa are much larger (>400 km in most cases) when compared to the surface winds (Figure 4j).

#### 3.2.4. Surface Fluxes

Generally, the variability of surface fluxes in convective environments over land is larger than that over water (Figures 4h and 4i). Surface fluxes are strongly impacted by land/ocean surface properties (surface temperature, roughness, etc.) which vary considerably more over land. Moreover, the parameterizations in the RAMS model do not account for changes in sea roughness with wind speeds. Surface flux variograms for some tropical land cases have relatively well-defined ranges. This is similar to the surface wind variograms (Figure 4c) and indicates the role of local processes in producing this variability in surface fluxes. The length scales range from 50 to 90 km

for most simulations, with secondary scales larger than 500 km also present in some simulations (Figure 4j). The multiple scales of variability in surface fluxes for certain simulations appear to be due to the presence of both land and ocean in these simulations.

#### 3.2.5. CAPE

Maximum convective available potential energy (MCAPE, Colman, 1990) variograms show that the Argentina simulations have the largest variability across most spatial scales; only Brazil1 and Congo (tropical land environments with isolated convection) have larger variability at scales less than ∼50 km. The effective length scales associated with MCAPE range from approximately 60 km in the Congo to around 600 km in Australia (Figure 4j). These scales may influence the spatial extent and organization of subsequent convective activity.

## 4. Summary and Conclusions

In this study, we use structure functions, specifically first-order structure function and variograms (which are proportional to second-order SF), to quantify horizontal spatial variability (both spatial roughness and variability magnitude) of several convectively important parameters in a wide variety of simulated tropical and subtropical convective environments. We find that:

- For near-surface fields, horizontal wind speed is the roughest (shorter correlation lengths) for length scales between 10 and 100 km over land.
- Tropical oceanic environments show the lowest magnitudes of variability in surface moisture and temperature, while subtropical land environments show the greatest variability across scales.
- On an average, the magnitude of mid-level moisture (500 hPa) variability over tropical oceanic convective environments is greater than that over tropical land and subtropical regions, pointing to the importance of strong large-scale moisture gradients in these environments.
- Certain variograms of near-surface wind speed and surface sensible and latent heat fluxes, show relatively well-defined ranges, implying sharp decorrelation lengths and a larger role of local processes, such as topography, in producing spatial variability.

Similar conclusions can be drawn from WRF output (Figures S2–S5 in Supporting Information S1). The above conclusions point to significant horizontal variability within tropical and subtropical convective environments with wide-ranging correlation length scales. Model grid spacings and observation densities that may be adequate for capturing most of the spatial variability for one variable may be inadequate for another variable. The length scales presented in this study can help guide the resolution requirements for large-domain model simulations and remotely sensed and in situ observational platforms. Furthermore, the scaling behavior of structure functions can be used to model sub-grid variability across length scales, conditioned upon the variable, altitude, convective regime, etc. This information is valuable in developing scale-aware parameterizations and stochastic parameterizations for coarse-resolution models. For example, stochastic parameterizations of sub-grid cloud fraction for global climate models can use the scaling exponents and length scales of water species mixing ratio fields from higher-resolution simulations, such as the ones used in this study, as constraints to inject more realistic, spatially coherent perturbations at unresolved scales. Finally, we emphasize that these results are obtained from high-resolution model output. The next step is to thoroughly verify these results by conducting the same analysis of observations.

## Conflict of Interest

The authors declare no conflicts of interest relevant to this study.

## Data Availability Statement

The code and data needed to produce the figures shown in this manuscript are available at Zenodo via Singh (2025). The code and simulation namelists for RAMS and WRF are available at Zenodo via P. Marinescu et al. (2025) and Bukowski et al. (2025), respectively.

**Acknowledgments**
This work is supported by INCUS, a NASA Earth Venture Mission, funded by NASA's Science Mission Directorate and managed through the Earth System Science Pathfinder Program Office under Contract 80LARC22DA011. Computational resources were provided by the NASA High-End Computing (HEC) Program through the NASA Advanced Supercomputing (NAS) Division at Ames Research Center. The manuscript benefitted from helpful discussions with Aaron Dunton and Jesse Loveridge and from insightful suggestions by two anonymous reviewers.

## References

Berner, J., Achatz, U., Batté, L., Bengtsson, L., Cámara, A. D., Christensen, H. M., et al. (2017). Stochastic parameterization: Toward a new view of weather and climate models. *Bulletin of the American Meteorological Society*, *98*(3), 565–588. https://doi.org/10.1175/BAMS-D-15-00268.1

Bukowski, J., Singh, I., Marinescu, P. , & van den Heever, S. C. (2025). WRF (Weather Research and Forecasting) model for the NASA INCUS mission (version V1.0) [Computer software]. *Zenodo*. https://doi.org/10.5281/ZENODO.16944997

Chilès, J.-P., & Delfiner, P. (2012). *Geostatistics: Modeling spatial uncertainty*. Wiley.

Colman, B. R. (1990). Thunderstorms above frontal surfaces in environments without positive CAPE. Part I: A climatology. *Monthly Weather Review*, *118*(5), 1103–1122. https://doi.org/10.1175/1520-0493(1990)118<1103:TAFSIE>2.0.CO;2

Cotton, W. R., Pielke, R. A. Sr., Walko, R. L., Liston, G. E., Tremback, C. J., Jiang, H., et al. (2003). RAMS 2001: Current status and future directions. *Meteorology and Atmospheric Physics*, *82*(1), 5–29. https://doi.org/10.1007/s00703-001-0584-9

Davison, J. L., Rauber, R. M., Girolamo, L. D., & LeMone, M. A. (2013). A revised conceptual model of the tropical marine boundary layer. Part I: Statistical characterization of the variability inherent in the wintertime trade wind regime over the Western tropical Atlantic. *Journal of the Atmospheric Sciences*, *70*(10), 3005–3024. https://doi.org/10.1175/jas-d-12-0321.1

Dolan, B., Kollias, P., van den Heever, S. C., Rasmussen, K. L., Oue, M., Luke, E., et al. (2023). Time resolved reflectivity measurements of convective clouds. *Geophysical Research Letters*, *50*(22), e2023GL105723. https://doi.org/10.1029/2023GL105723

Fabry, F. (2006). The spatial variability of moisture in the boundary layer and its effect on convection initiation: Project-long characterization. *Monthly Weather Review*, *134*(1), 79–91. https://doi.org/10.1175/mwr3055.1

Fischer, L., Craig, G. C., & Kiemle, C. (2013). Horizontal structure function and vertical correlation analysis of mesoscale water vapor variability observed by airborne lidar. *Journal of Geophysical Research: Atmospheres*, *118*(14), 7579–7590. https://doi.org/10.1002/jgrd.50588

Freischem, L. J., Weiss, P., Christensen, H. M., & Stier, P. (2024). Multifractal analysis for evaluating the representation of clouds in global kilometer-scale models. *Geophysical Research Letters*, *51*(20), e2024GL110124. https://doi.org/10.1029/2024GL110124

Grant, L. D., Kirsch, B., Bukowski, J., Falk, N. M., Neumaier, C. A., Sakradzija, M., et al. (2024). How variable are cold pools? *Geophysical Research Letters*, *51*(6), e2023GL106784. https://doi.org/10.1029/2023gl106784

Hurst, H. E. (1956). Methods of using long-term storage in reservoirs. *Proceedings - Institution of Civil Engineers*, *5*(5), 519–543. https://doi.org/10.1680/iicep.1956.11503

Kahn, B. H., Teixeira, J., Fetzer, E. J., Gettelman, A., Hristova-Veleva, S. M., Huang, X., et al. (2011). Temperature and water vapor variance scaling in global models: Comparisons to satellite and aircraft data. *Journal of the Atmospheric Sciences*, *68*(9), 2156–2168. https://doi.org/10.1175/2011JAS3737.1

Khintchine, A. (1934). Korrelationstheorie der stationären stochastischen Prozesse. *Mathematische Annalen*, *109*(1), 604–615. https://doi.org/10.1007/BF01449156

Kiemle, C., Groß, S., Wirth, M., & Bugliaro, L. (2017). Airborne lidar observations of water vapor variability in tropical shallow convective environment. *Surveys in Geophysics*, *38*(6), 1425–1443. https://doi.org/10.1007/s10712-017-9431-5

Lewis, G. M., Austin, P. H., & Szczodrak, M. (2004). Spatial statistics of marine boundary layer clouds. *Journal of Geophysical Research*, *109*(D4), D04104. https://doi.org/10.1029/2003JD003742

Madaus, L. E., & Hakim, G. J. (2016). Observable surface anomalies preceding simulated isolated convective initiation. *Monthly Weather Review*, *144*(6), 2265–2284. https://doi.org/10.1175/mwr-d-15-0332.1

Marinescu, P. J., van den Heever, S., Grant, L. D., Bukowski, J., & Singh, I. (2024). How much convective environment subgrid spatial variability is missing within atmospheric reanalysis datasets?

Marinescu, P., Freeman, S. W., Grant, L. D., Saleeby, S. M., Leung, G., Bukowski, J., et al. (2025). RAMS (Regional Atmospheric Modeling System) for the NASA INCUS mission (version v0.1) [Computer software]. *Zenodo*. https://doi.org/10.5281/ZENODO.16944888

Marzban, C., & Sandgathe, S. (2009). Verification with variograms. *Weather and Forecasting*, *24*(4), 1102–1120. https://doi.org/10.1175/2009waf2222122.1

Nastrom, G. D., Jasperson, W. H., & Gage, K. S. (1986). Horizontal spectra of atmospheric tracers measured during the Global Atmospheric Sampling Program. *Journal of Geophysical Research*, *91*(D12), 13201–13209. https://doi.org/10.1029/JD091iD12p13201

Naumann, A. K., & Kiemle, C. (2020). The vertical structure and spatial variability of lower-tropospheric water vapor and clouds in the trades. *Atmospheric Chemistry and Physics*, *20*(10), 6129–6145. https://doi.org/10.5194/acp-20-6129-2020

Prasanth, S., Haddad, Z. S., Sawaya, R. C., Sy, O. O., van den Heever, M., Narayana Rao, T., & Hristova-Veleva, S. (2023). Quantifying the vertical transport in convective storms using time sequences of radar reflectivity observations. *Journal of Geophysical Research: Atmospheres*, *128*(10), e2022JD037701. https://doi.org/10.1029/2022jd037701

Saleeby, S. M., & van den Heever, S. C. (2013). Developments in the CSU-RAMS aerosol model: Emissions. *Nucleation, Regeneration, Deposition, and Radiation*, *52*(12), 2601–2622. https://doi.org/10.1175/JAMC-D-12-0312.1

Schemann, V., Stevens, B., Grützun, V., & Quaas, J. (2013). Scale dependency of total water variance and its implication for cloud parameterizations. *Journal of the Atmospheric Sciences*, *70*(11), 3615–3630. https://doi.org/10.1175/JAS-D-13-09.1

Schulte, R. M., Chase, R. J., Dolan, B., Marinescu, P. J., Posselt, D. J., Rasmussen, K. L., & van den Heever, S. C. (2024). Unclouding the correlations: A principal component analysis of convective environments. *Geophysical Research Letters*, *51*(24), e2024GL111732. https://doi.org/10.1029/2024GL111732

Selz, T., Fischer, L., & Craig, G. C. (2017). Structure function analysis of water vapor simulated with a convection-permitting model and comparison to airborne lidar observations. https://doi.org/10.1175/JAS-D-16-0160.1

Sherwood, S. C. (1996). Maintenance of the free-tropospheric tropical water vapor distribution. Part I: Clear regime budget. *Journal of Climate*, *9*(11), 2903–2918. https://doi.org/10.1175/1520-0442(1996)009<2903:MOTFTT>2.0.CO;2

Singh, I. (2025). Horizontal_spatial_variability (version 1.0.1). https://doi.org/10.5281/zenodo.15843888

Skamarock, W., Klemp, J. B., Dudhia, J., Gill, D. O., Liu, Z., Berner, J., et al. (2019). A description of the advanced research WRF model version 4.1. https://doi.org/10.5065/1dfh-6p97

Smith, D. F., Gasiewski, A. J., Jackson, D. L., & Wick, G. A. (2005). Spatial scales of tropical precipitation inferred from TRMM microwave imager data. *IEEE Transactions on Geoscience and Remote Sensing*, *43*(7), 1542–1551. https://doi.org/10.1109/tgrs.2005.848426

Stevens, B., Ament, F., Bony, S., Crewell, S., Ewald, F., Gross, S., et al. (2019). A high-altitude long-range aircraft configured as a cloud observatory: The NARVAL expeditions. *Bulletin of the American Meteorological Society*, *100*(6), 1061–1077. https://doi.org/10.1175/BAMS-D-18-0198.1

Storer, R. L., & Posselt, D. J. (2019). Environmental impacts on the flux of mass through deep convection. *Quarterly Journal of the Royal Meteorological Society*, *145*(725), 3832–3845. https://doi.org/10.1002/qj.3669

Tompkins, A. M. (2002). A prognostic parameterization for the subgrid-scale variability of water vapor and clouds in large-scale models and its use to diagnose cloud cover. *Journal of the Atmospheric Sciences*, *59*(12), 1917–1942. https://doi.org/10.1175/1520-0469(2002)059<1917:APPFTS>2.0.CO;2

Tompkins, A. M., & Berner, J. (2008). A stochastic convective approach to account for model uncertainty due to unresolved humidity variability. *Journal of Geophysical Research*, *113*(D18), D18101. https://doi.org/10.1029/2007JD009284

Tsonis, A. A., Roebber, P. J., & Elsner, J. B. (1999). Long-range correlations in the extratropical atmospheric circulation: Origins and implications. *Journal of Climate*, *12*(5), 1534–1541. https://doi.org/10.1175/1520-0442(1999)012<1534:LRCITE>2.0.CO;2

Tung, K. K., & Orlando, W. W. (2003). The $k^{-3}$ and $k^{-5/3}$ energy spectrum of atmospheric turbulence: Quasigeostrophic two-level model simulation. *Journal of the Atmospheric Sciences*, *60*(6), 824–835. https://doi.org/10.1175/1520-0469(2003)060<0824:TKAKES>2.0.CO;2

van den Heever, S. C. (2021). *NASA selects new mission to study storms, impacts on climate models*. NASA Earth. Retrieved from https://www.nasa.gov/press-release/nasa-selects-new-mission-to-study-storms-impacts-on-climate-models

van den Heever, S. C., Saleeby, S. M., Grant, L. D., Igel, A. L., & Freeman, S. W. (2023). *RAMS - The regional atmospheric modeling system (version v6.3.04)*. Zenodo. https://doi.org/10.5281/zenodo.8327421

Zhang, F., Snyder, C., & Rotunno, R. (2003). Effects of moist convection on mesoscale predictability. Retrieved from https://journals.ametsoc.org/view/journals/atsc/60/9/1520-0469_2003_060_1173_eomcom_2.0.co_2.xml

## References From the Supporting Information

Germann, U., & Joss, J. (2001). Variograms of radar reflectivity to describe the spatial continuity of alpine precipitation. *Journal of Applied Meteorology*, *40*(6), 1042–1059. https://doi.org/10.1175/1520-0450(2001)040<1042:vorrtd>2.0.co;2

Jensen, M. P., Flynn, J. H., Judd, L. M., Kollias, P., Kuang, C., Mcfarquhar, G., et al. (2022). A succession of cloud, precipitation, aerosol, and air quality field experiments in the coastal urban environment. *Bulletin of the American Meteorological Society*, *103*(2), 103–105. https://doi.org/10.1175/BAMS-D-21-0104.1

Lu, C., & Koch, S. E. (2008). Interaction of upper-tropospheric turbulence and gravity waves as obtained from spectral and structure function analyses. *Journal of the Atmospheric Sciences*, *65*(8), 2676–2690. https://doi.org/10.1175/2007JAS2660.1

Nesbitt, S. W., Salio, P. V., Ávila, E., Bitzer, P., Carey, L., Chandrasekar, V., et al. (2021). A storm safari in subtropical South America: Proyecto RELAMPAGO. *Bulletin of the American Meteorological Society*, *102*(8), E1621–E1644. https://doi.org/10.1175/bams-d-20-0029.1

Pressel, K. G., & Collins, W. D. (2012). First-order structure function analysis of statistical scale invariance in the AIRS-observed water vapor field. *Journal of Climate*, *25*(16), 5538–5555. https://doi.org/10.1175/JCLI-D-11-00374.1

Ryu, D., & Famiglietti, J. S. (2006). Multi-scale spatial correlation and scaling behavior of surface soil moisture. *Geophysical Research Letters*, *33*(8), L08404. https://doi.org/10.1029/2006gl025831

Sobel, A. H., Sprintall, J., Maloney, E. D., Martin, Z. K., Wang, S., de Szoeke, S. P., et al. (2021). Large-scale state and evolution of the atmosphere and ocean during PISTON 2018. *Journal of Climate*, *34*(12), 5017–5035. https://doi.org/10.1175/JCLI-D-20-0517.1

Thompson, D. R., Kahn, B. H., Brodrick, P. G., Lebsock, M. D., Richardson, M., & Green, R. O. (2021). Spectroscopic imaging of sub-kilometer spatial structure in lower-tropospheric water vapor. *Atmospheric Measurement Techniques*, *14*(4), 2827–2840. https://doi.org/10.5194/amt-14-2827-2021

Voss, S., Zimmermann, B., & Zimmermann, A. (2016). Detecting spatial structures in throughfall data: The effect of extent, sample size, sampling design, and variogram estimation method. *Journal of Hydrology*, *540*, 527–537. https://doi.org/10.1016/j.jhydrol.2016.06.042